In-situ observations and modeling of spring snowmelt processes in an Altay Mountains river basin

Article *in* Journal of Applied Remote Sensing · April 2014

DOI: 10.1117/1.JRS.8.084697

5 authors, including:

Xuejiao Wu
Chinese Academy of Sciences

Ninglian Wang
Chinese Academy of Sciences

Yongping Shen
Cold and Arid Regions Environmental and Engineering Research Institute Chinese A…

Wei Zhang
Chinese Academy of Sciences

Journal of
Applied Remote Sensing

In-situ observations and modeling of spring snowmelt processes in an Altay Mountains river basin

Xuejiao Wu
Ninglian Wang
Yongping Shen
Jianqiao He
Wei Zhang

In-situ observations and modeling of spring snowmelt processes in an Altay Mountains river basin

Xuejiao Wu,[a,b,*] Ninglian Wang,[a] Yongping Shen,[a] Jianqiao He,[a] and Wei Zhang[a,b]

[a]Cold and Arid Regions Environmental and Engineering Research Institute, Chinese Academy of Sciences, State Key Laboratory of Cryospheric Sciences, Lanzhou, Gansu 730000, China
[b]University of Chinese Academy of Sciences, Beijing 100049, China

Abstract. Snowmelt is a principal source for ground-water recharge and stream flows in mountainous regions of northwestern China. Knowledge of the timing, magnitude, and processes of snowmelt under changing climate conditions is required for appropriate water resource management. The Utah energy balance (UEB) model was used to simulate the development and melting of spring (March 2012) snow cover at an observation site in the Kayiertesi River Basin in the Altay Mountains in Xinjiang. The modeled results were validated by field measurements and remotely sensed data. Results show that the simulation of the snowmelt process lasted for 24 days and the modeled snow water equivalent (SWE) closely matched the observed SWE, with a mean relative error of 7.2%. During the snowmelt process, net radiation was the major energy source of the snow layer. The variation of the snowmelt outflow was closely related to the snowmelt amounts and air temperature. The initial results of this modeling process show that our calibrated parameters were reasonable and the UEB model can be used for simulating and forecasting peak snowmelt outflows in this region. © *2014 Society of Photo-Optical Instrumentation Engineers (SPIE)* [DOI: 10.1117/1.JRS.8.084697]

Keywords: snow water equivalent; sensible heat flux; latent heat flux; snow cover; outflow.

Paper 14037SS received Jan. 15, 2014; revised manuscript received Mar. 10, 2014; accepted for publication Mar. 27, 2014; published online Apr. 25, 2014.

1 Introduction

Snowmelt is an important source of fresh water and is a critical water resource in the mountain regions of northwestern China and other similar regions of the world. Spring snowmelt water is a major source of river runoff, which can support the demand for water resources in oases, ease droughts that affect oasis agriculture, and meet the demands of spring irrigation. However, rapid spring snowmelt can cause flood disasters that can endanger public and personal property and safety.[1,2] Recently, frequent extreme weather events caused snowmelt flood disasters that ground much of normal life to a halt. For instance, in January 2010, snowstorms and snowmelt flooding occurred in 12 counties of the Tacheng-Altay regions of northwestern China, affecting more than 90,000 people.[3] In the context of global warming, changes in snow hydrological processes also had significant economic impacts on the development of northwestern China. Therefore, the work of monitoring snow changes, modeling snowmelt processes, and forecasting snowmelt outflows and runoff is important for appropriate water resource management and flood prevention.

Current snowmelt models can generally be classified into two categories: empirical temperature-index models[4,5] (such as the degree-day model[6]) and physically based energy-balance models.[7] The degree-day model has been widely used in Greenland, northern Europe, the Qinghai-Tibet Plateau, and other regions for snow and ice melting process studies.[8–10] The degree-day method has also been integrated into other hydrological models, such as the snowmelt runoff model[11] and the Hydrologiska Byrans Vattenbalansavdelning model developed in Sweden.[12] However, in some cases, the degree-day model cannot simulate ideal results because it

*Address all correspondence to: Xuejiao Wu, E-mail: wxjiao608@126.com

only considers the air temperature factor. Many attempts have been made to improve the original degree-day model by incorporating more variables, such as direct solar radiation.[13,14]

Energy-balance models use physically based calculations of heat exchanges without a strong regional dependency. They can describe energy exchanges in detail at the snow-air interface and can produce relatively accurate simulations and predictions of snowmelt conditions. Based on the theory of energy balance, certain snowmelt models have been developed, such as the SNOWPACK model which can handle the special problems of avalanche warning by considering the mechanical structure of snow layers in detail.[15] The prairie blowing snow model takes into account the transport of blowing snow, sublimation, and other weather conditions.[16] Simultaneous heat and water model focuses on interpreting the relationship between snow and solid-frozen soil.[17] The single-layer Utah energy balance (UEB) model is a simple snowmelt model with a small number of state variables and adjustable parameters, which avoids the need for extensive assumptions and parameterizations.[18] It is transportable and applicable in many different locations without needing much calibration.[19] Other hydrological models that have deeply integrated energy-balance snowmelt models are Système Hydrologique Européen (SHE),[20] Soil and Water Assessment Tool (SWAT),[21] and the distributed hydrology soil vegetation model (DHSVM).[22]

In this study, the UEB snowmelt model was used for snowmelt modeling at a site in Altay Mountains in Xinjiang. The aims of the study were (1) to evaluate the feasibility of the UEB model in our study area and (2) to explore the variability of the SWE, outflow, and flux components in our study site during a spring snowmelt period.

2 Study Sites and Data

Our study area was located in the Kayiertesi River Basin in the Altay Mountains of northern Xinjiang; this basin is the headwater source of Eerqisi River (Fig. 1). The climate of this region is influenced by the westerly airflow, and most of the annual precipitation is in the form of snow which creates a thick and stable snow cover during the winter. The drainage area of this basin is 2350 km^2 with an altitude ranging from 1159 to 3846 m a.s.l. The area has a cool climate with a multiyear mean annual temperature of 3.0°C from 1962 to 2012. Snowmelt begins to melt in March (with a monthly mean temperature of −6.3°C) in the study area. The multiyear mean annual precipitation is 190.7 mm from 1962 to 2012, and the two minimum months are February (8.1 mm) and March (10.5 mm). Our open observation site is located at the Kuwei Hydrologic Station in the outlet of the basin, at 47°20′N, 89°41′E with an elevation of 1370 m. Field measurements at the site include meteorological measurements, certain snow properties, and frozen soil monitoring. The meteorological measurements include air temperature (±0.4°C), relative humidity (±2%) (HMP45C probe, Vaisala, Helsinki, Finland), and wind speed ($\pm 0.3\ m\,s^{-1}$) and direction (Propvane-05103 anemometer, RM Young, Traverse City, Michigan) at a height of 3 m above the ground surface.

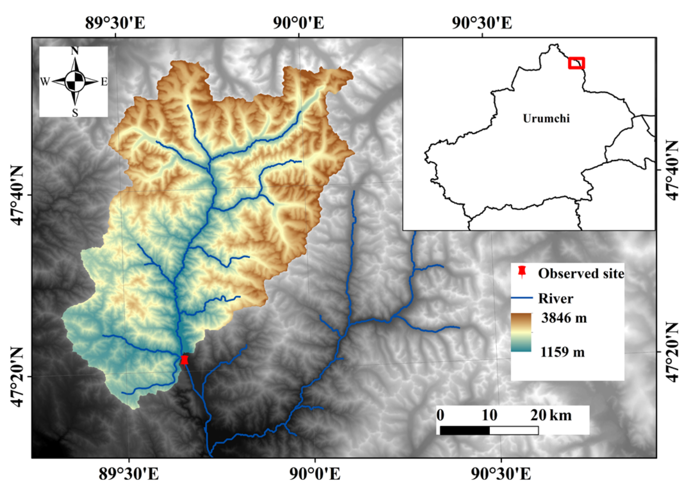

Fig. 1 Map of study area.

The snow properties measurements include snow depth (±1 cm) (Campbell SR50A snow depth sensor, Campbell Scientific, Logan, Utah), snow water equivalent (SWE) (snow pillow), and the layered snow temperature (±0.5°C) (Campbell SI-111 infrared radiometer, Campbell Scientific). Solid precipitation was measured in mm water equivalent (mm w.e., ±0.1%) using a Geonor T-200B (Augusta, New Jersey) accumulative weighing bucket precipitation gauge without heating. All sensors were connected to a data logger (CR1000, Campbell Scientific), and the automatic weather station recorded the half-hourly mean of the measurements taken every 10 s. Other parameters such as layered soil temperature and soil moisture were also monitored. Four new net radiometers (±1%) (CNR4, Kipp & Zonen, Delft, The Netherlands) were installed at the Kuwei Hydrologic Station in September, 2013 to monitor air incident and reflected short-wave radiation (S↓ and S↑) and incoming and outgoing long-wave radiation (L↓ and L↑).

In order to validate our modeled results, we used MOD10A1 daily snow cover products which spatially mapped snow cover variations in the Kayiertesi River Basin from March to June 2012. MOD10A1 daily products are available from the National Snow and Ice Data Center (NSIDC, Boulder, Colorado), and include snow extent, snow albedo, fractional snow cover, and quality assessment data at 500-m resolution, gridded in a sinusoidal map projection. Cloud pixels were determined by daily snow cover series, and snow cover mapping was made by compositing 3 to 5 days of the MOD10A1 product to find the maximum snow cover extent during 5 days. The intent of the algorithm in our study was similar to that of MOD10A2, which maximizes the number of snow pixels while minimizing the number of cloud pixels.[23,24]

3 Model Description

The UEB snow model is an energy-balance snow accumulation and melt model which uses a lumped representation of the snowpack and keeps track of the water and energy balance. It was developed in the mid-1990s by David Tarboton's research group[25] and has been updated over the years. The model is driven by inputs of precipitation, air temperature, relative humidity, wind speed, and radiation at hourly steps sufficient to detect the diurnal cycle. The melt outflow uses Darcy's law, and it is a function of the liquid fraction. This allows the model to account for continued outflow even when the energy balance is negative.

The snowpack is characterized by two primary state variables in the model, energy content [U (kJ m^{-2})] and water equivalent [W(m)]. U and W are defined per unit of horizontal area. The energy content, U, is defined relative to a reference state of water at 0°C and contains no liquid water. These two state variables are solved by the following energy- and mass-balance equations:

$$dU/dt = Q_{sn} + Q_{li} + Q_p + Q_g + Q_h + Q_e - Q_{le} - Q_m, \tag{1}$$

where the unit of all terms is kJ m^{-2} h^{-1}. Q_{sn} represents the net solar radiation, Q_{li} represents the incoming long-wave radiation, Q_p represents the advected heat from precipitation, Q_g represents the ground heat flux, Q_h and Q_e represent the sensible heat flux and the latent heat flux, respectively, Q_{le} represents the outgoing long-wave radiation, and Q_m represents the heat advected with melt water, and

$$dW/dt = P_r + P_s - M_r - E, \tag{2}$$

where the unit of all terms is m h^{-1}. P_r and P_s represent the rate of precipitation as rain and snow, respectively, M_r represents the melt rate, and E represents the sublimation rate. The theory of the model is more completely described in Ref. 26.

Long-wave radiations were parameterized using the Stefan–Boltzmann law. Net short-wave radiation was calculated as

$$Q_{sn} = Q_{si}(1 - a), \tag{3}$$

where a is calculated as a function of solar illumination angle and snow surface age.[27] Incident short-wave radiation is estimated from diurnal temperature range (DTR) and taken as[28]

$$Q_{\mathrm{si}} = T_{\mathrm{f}} I_{\mathrm{o}} \mathrm{HRI}, \tag{4}$$

where T_{f} is an atmospheric transmittance, I_{o} is the solar constant ($4914\ \mathrm{kJ\,m^{-2}\,h^{-1}}$), and HRI is a multiplication factor relative to the integral of the illumination angle. In the process of parameterization of HRI, local horizons, azimuth, and slope were used to find local sunrise and sunset times and integrate solar radiation received on the slope for each time step. T_{f} was determined by the DTR.

The measured precipitation rate, P, was composed of rain, P_{r}, and snow, P_{s}, using the following calculation based on air temperature, T_{a}:

$$\begin{aligned} &P_{\mathrm{r}} = P \qquad T_{\mathrm{a}} \geq T_{\mathrm{r}}, \\ &P_{\mathrm{r}} = P(T_{\mathrm{a}} - T_{\mathrm{b}})/(T_{\mathrm{r}} - T_{\mathrm{b}}) \qquad T_{\mathrm{b}} < T_{\mathrm{a}} < T_{\mathrm{r}}, \end{aligned} \tag{5}$$

$$P_{\mathrm{r}} = 0 \qquad T_{\mathrm{a}} \leq T_{\mathrm{b}}, \quad P_{\mathrm{s}} = (P - P_{\mathrm{r}})\,F, \tag{6}$$

where T_{r} and T_{b} are the threshold air temperatures to distinguish rain and snow. F represents a snow drift factor, which depends on local topography.[29] The temperature of rain is accounted as the higher temperature of freezing point and the air temperature, and the temperature of snow is the lower temperature of the freezing point and the air temperature. In order to convert the precipitation to the reference state (0°C ice phase), the advected heat is required

$$Q_{\mathrm{p}} = P_{\mathrm{s}} C_{\mathrm{s}} \rho_{\mathrm{w}}\ \min(T_{\mathrm{a}}, 0) + P_{\mathrm{r}}[h_{\mathrm{f}} \rho_{\mathrm{w}} + C_{\mathrm{w}} \rho_{\mathrm{w}}\ \max(T_{\mathrm{a}}, 0)], \tag{7}$$

where C_{s} is the specific heat of ice ($2.09\ \mathrm{kJ\,kg^{-1}\,°C^{-1}}$) and C_w is the specific heat of water ($4.18\ \mathrm{kJ\,kg^{-1}\,°C^{-1}}$), h_{f} is the heat of fusion ($333.5\ \mathrm{kJ\,kg^{-1}}$), and ρ_{w} is the density of water ($1000\ \mathrm{kg\,m^{-3}}$).

Sensible heat fluxes between the air and snow surface were modeled using the concept of flux proportional to temperature gradient as follows:

$$Q_{\mathrm{h}} = K_{\mathrm{h}} \rho_{\mathrm{a}} C_{\mathrm{p}} (T_{\mathrm{a}} - T_{\mathrm{s}}), \tag{8}$$

where K_{h} is the heat conductance ($\mathrm{m\,h^{-1}}$), ρ_{a} is the air density determined from atmospheric pressure and temperature, C_{p} is the air specific heat capacity ($1.005\ \mathrm{kJ\,kg^{-1}\,°C^{-1}}$), and T_{s} is the snow surface temperature. The parameterization of T_{s} is complicated; it correlates to the surface conductivity, snow density, air vapor pressure, and other parameters involved in the surface energy balance.[22]

For latent heat fluxes, the vapor pressure gradient is the key influencing factor:

$$Q_{\mathrm{e}} = -h_{\mathrm{v}} M_{\mathrm{e}} = K_{\mathrm{e}} h_{\mathrm{v}} 0.622/R_{\mathrm{d}} T_{\mathrm{a}} [e_{\mathrm{a}} - e_{\mathrm{s}}(T_{\mathrm{s}})], \tag{9}$$

$$M_{\mathrm{e}} = K_{\mathrm{e}} \rho_{\mathrm{a}} (q_{\mathrm{s}} - q), \tag{10}$$

$$K_{\mathrm{h}} = K_{\mathrm{e}} = K_{\mathrm{neutral}} = k^2 V / [\ln(z/z_0)]^2, \tag{11}$$

where M_{e} is the vapor transport away from the surface ($\mathrm{kg\,h^{-1}}$), h_{v} is the latent heat of sublimation ($2834\ \mathrm{kJ/kg}$), e_{a} and e_{s} are the air vapor pressure and vapor pressure at the snow surface, respectively, R_{d} is the dry gas constant ($287\ \mathrm{J\,kg^{-1}\,K^{-1}}$), K_{e} is the vapor conductance ($\mathrm{m\,h^{-1}}$), and q_{s} and q are the surface specific humidity and specific humidity (kg water vapor/kg air), respectively. V is the wind speed ($\mathrm{m\,h^{-1}}$) at height z(m), z_0 is roughness height at which the logarithmic boundary layer profile predicts zero velocity (m), and k is von Karman's constant (0.4). Thus, the water equivalence depth of sublimation is

$$E = -Q_{\mathrm{e}} / \rho_{\mathrm{w}} h_{\mathrm{v}}. \tag{12}$$

The outflow rate is determined by the energy content state variable U and Darcy's law for flow through porous media

$$M_{\mathrm{r}} = K_{\mathrm{sat}} S^{*3}, \tag{13}$$

where K_{sat} is the snow saturated hydraulic conductivity and S^* is the relative saturation in excess of water retained by capillary forces (based on Male[30]). Thus the heat advected with the outflow is

$$Q_m = \rho_w h_v M_r. \tag{14}$$

4 Results and Discussion

4.1 *Parameters and Input Data*

Simulations were performed for the period of March 1–31, 2012. We estimated the radiation and snowmelt in the open area using hourly meteorological inputs of precipitation, temperature, wind speed, and relative humidity. Although interception and sublimation may be the primary processes during the early snow season, our simulation period was chosen to cover the melt period only, because the simulating and forecasting peak snowmelt flow is the main focus of this paper. For the area, the meteorological variables are assumed to be representative of conditions at a height of 3 m above the ground. The input meteorological data and the site initial parameter data were obtained from the measurement in the study area. The area was covered by snow from November 2011 to March 2012, and the snow accumulated to a maximum depth of 0.4 m with maximum water equivalent of 0.06 m in February.

Table 1 summarizes the observed site characteristics and initial status of the snow. The slope and aspect were calculated based on 30-m digital elevation model (DEM). The Kuwei observation site has a flat surface with respect to the upper parts of the basin. The initial SWE (0.06 m) was defined by snow depth data. Table 2 lists the adjustable and the fixed parameters used in the UEB model. Some of the calibrated parameters were different from the recommended values in the model, including surface aerodynamic roughness, infrared-band and visible-band reflectance, and average snow density. Surface aerodynamic roughness (Z_0) is a quite sensitive parameter in the model, which directly affects the heat transport between air and the surface. From existing research results, the surface aerodynamic roughness of the snow is usually around 0.001 m.[31] Herein, we adopted 0.0009 m from the results of Sun et al.[32] New snow near-infrared band and visible-band reflectance came from field observations using an Analytical Spectral Devices (ASD) spectrograph (FieldSpec 3, Analytical Spectral Devices, Inc., Boulder, Colorado) in Xinjiang. From site snow observations, an average snow density of 150 kg/m^3 was given in the model. The temperature T_r above which precipitation is rain and the snow saturated hydraulic conductivity (K_{sat}) were adjusted (calibrated) based on the observed SWE at the central site. Other parameters followed the original UEB model.[19,25]

During the period of simulation, mean air temperatures ranged from −13.2°C to 2.7°C and there was a significant increasing trend (Fig. 2). Wind speed and relative humidity presented an obvious opposite change tendency (Fig. 2). Wind speed, which had a daily mean of 1.72 $m\,s^{-1}$ during the modeled period, played a significant role in the turbulent exchange between the atmosphere and the glacial surface. Relative humidity directly affected the latent heat flux exchange, with a daily mean of 0.56 during the modeled period. There was little precipitation during the snowmelt simulation period in this area. There was one snowfall on March 19 and the SWE was 0.1 mm w.e., which was the only time of precipitation in the modeled month.

Table 1 Site parameters.

Site variables	Values
Slope	5 deg
Aspect	48.5 deg
Latitude	47.33°N
Longitude	89.65°E
Initial SWE	0.06 m
Atmospheric pressure	85,600 Pa

Table 2 Snowmelt model fixed parameters.

Parameter	Values	Basis
Surface aerodynamic roughness (Z_0)	0.0009 m	Ref. 32
Snow saturated hydraulic conductivity (K_{sat})	$25\ m\,h^{-1}$	Adjusted
New snow near-infrared-band reflectance (a_{iro})	0.63	This study
New snow visible-band reflectance (a_{vo})	0.89	This study
Ground heat capacity (C_g)	$2.09\ kJ\,kg^{-1}\,°C^{-1}$	Ref. 26
Density of soil layer (r_g)	$1700\ kg\,m^{-3}$	Ref. 26
Snow density (r_s)	$150\ kg\,m^{-3}$	This study
Liquid holding capacity of snow (L_c)	0.05	Ref. 26
Temperature above which precipitation is rain (T_r)	1.2°C	Adjusted
Temperature below which precipitation is snow (T_s)	−1°C	Ref. 26
Wind/air temperature measurement height (z)	3 m	This study
Soil effective depth (D_e)	0.1 m	Ref. 26
Bare ground albedo (A_{bg})	0.25	Ref. 26
Nominal measurement of height for air temperature and humidity (z_{ms})	3 m	This study
Emissivity of snow (e_s)	0.98	Ref. 26
Thermal conductivity of surface snow (l_s)	$1\ kJ\,m^{-1}\,C^{-1}\,h^{-1}$	Ref. 19
Thermal conductivity of soil (l_g)	$4\ kJ\,m^{-1}\,C^{-1}\,h^{-1}$	Ref. 19

4.2 *Validation of Simulation*

The model was able to predict the SWE, snow surface temperature, radiation, energy fluxes, and outflow. The actual measurements of SWE and the surface temperature were available for the snowmelt simulation period in 2012, so the SWE comparisons serve as a comprehensive test of all aspects of a model. The SWE was derived from snow depths, together with snow density ($150\ kg/m^3$) by snow depth sensors mounted in the weather station. A fixed and average snow

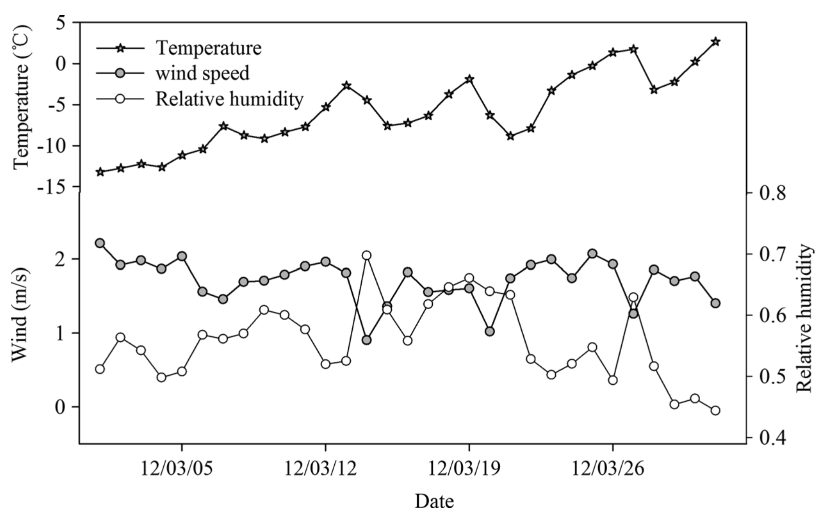

Fig. 2 Meteorological characteristics in snowmelt season (March).

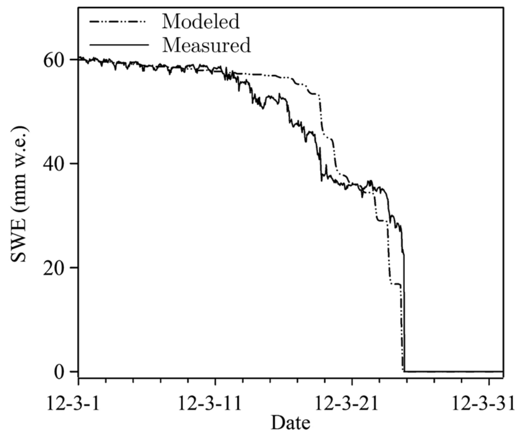

Fig. 3 Comparison between modeled and measured SWE.

density was chosen when calculating the SWE using initial measurements because snow density is a fixed parameter in the model. Comparison between the modeled SWEs and observations (Fig. 3) indicates that the main snowmelt was well modeled with a mean relative error of 7.2%, but some early snowmelt was not modeled very accurately. From the middle to the late snowmelt period, there was a generally better agreement. The SWE values and the snowmelt process at Kuwei observation site were reasonably predicted by the model.

The snowmelt process took about 24 days from March 1. This result was also validated with remote sensing data. The spring snowmelt persistence time was studied using MODIS images of 2012 at the Kuwei observation site. Table 3 presents the pixel analyses of MODIS images for March 2012, which covers the Kuwei observation site. Results show that there were eight cloudy days before March 24. Due to little precipitation during the snowmelt period, the cloud pixels can be considered as snow until March 24 by compositing from 3 to 5 days. The MODIS images well caught the dates on which the ground was covered by snow before March 25. Land was finally detected on April 5. The reason for the delay in detection of land can be due to high cloud cover from March 25 to April 4. We could not determine the actual ending time of the snowmelt because only one pixel covered our study site. To further verify how long the snow persisted in the study area during the snowmelt period, the spatial distributions of snow cover were mapped based on MOD10A1 data (Fig. 4). It can be seen that snow melted at higher and higher elevations over time because the temperature regularly decreased with increasing altitude. The basin was covered by snow on March 1 and by March 26 snow in the area along the river downstream of the basin had vanished. The range of altitude in the melt area on March 26 was between 1300 and 1450 m, which is consistent with the altitude of the Kuwei observation site (1370 m). Thus, from remote sensing data, we concluded that the snow had melted away by March 26 at Kuwei observation site and this result agreed well with our modeled result.

We then compared the modeled and the observed surface temperatures (T_s) at the hourly scale and the mean daily scale (Fig. 5). When the ground was covered by snow before March 24, the modeled surface temperatures were reasonably accurate in the daytime but were underestimated at night. After March 24, the modeled surface temperatures were overestimated in the daytime but were reasonably accurate at night when the ground soil was exposed [Fig. 5(a)]. These discrepancies might have been caused by the UEB model itself. In the UEB model, parameterization for surface temperature is a challenging physical problem that needs to incorporate the surface conductivity, snow density, air vapor pressure, and several other parameters involved in the surface energy balance. Moreover, when the surface is not snow-covered, the surface energy balance parameters change, and UEB was not really designed for nonsnow-covered situations (Dr. David Tarboton, personal communication). Nevertheless, the variability of the modeled mean daily T_s was very similar to that of the measured mean daily T_s, with a strong statistically significant positive correlation ($r = 0.93,\ p < 0.001$) [Fig. 5(b)].

Table 3 Summary of analyses for March 2012 at the Kuwei observation site from MODIS.

Date	MODIS10A1	Date	MODIS10A1
March 1, 2012	S	March 19, 2012	C
March 2, 2012	S	March 20, 2012	C
March 3, 2012	S	March 21, 2012	C
March 4, 2012	S	March 22, 2012	C
March 5, 2012	S	March 23, 2012	S
March 6, 2012	C	March 24, 2012	S
March 7, 2012	C	March 25, 2012	C
March 8, 2012	S	March 26, 2012	C
March 9, 2012	S	March 27, 2012	C
March 10, 2012	S	March 28, 2012	C
March 11, 2012	C	March 29, 2012	C
March 12, 2012	S	March 30, 2012	C
March 13, 2012	S	March 31, 2012	C
March 14, 2012	S	April 1, 2012	C
March 15, 2012	S	April 2, 2012	C
March 16, 2012	S	April 3, 2012	C
March 17, 2012	C	April 4, 2012	C
March 18, 2012	S	April 5, 2012	L

Note: S, snow; C, cloud, and L, land.

4.3 *Surface Energy Flux*

Incoming short-wave and long-wave radiation during the simulation period is shown in Fig. 6. The mean solar energy resource value was 223.3 $\mathrm{W/m^2}$ in March, 2012, which was close to the maximum of the Tanggula region, 249 $\mathrm{W/m^2}$.[33] It followed an orderly daily cycle process, with the mean daily values of short-wave radiation varying from 110.5 to 290 $\mathrm{W/m^2}$ [Fig. 6(a)]. There were 4 days when the short-wave radiation was only half of that on other days. Coincidentally, the incoming long-wave radiation presented higher values in those days [Fig. 6(b)]. The long-wave radiation showed a slight increase during the snowmelt period, with a monthly mean value of 226.7 $\mathrm{W/m^2}$ in March. The daily mean incoming long-wave radiation varied between 181.8 and 321 $\mathrm{W/m^2}$, which was caused by incoming radiation being affected by cloud cover.

Figure 7 illustrates hourly variations of the modeled heat fluxes, including sensible heat flux (H), latent heat flux (LE), and net radiation (R_n) between the surface and the atmosphere above. The daily mean values of H varied between −7 and 1.83 $\mathrm{W/m^2}$ from March 1 to 24. H was negative in the daytime and positive at night, indicating that air temperature was lower than surface temperature in the daytime but higher than the latter at night [Fig. 7(a)]. This demonstrates that heat was transferred from the snow surface to the atmosphere in the daytime and from the atmosphere to the snow surface at night. This result agreed well with the previous research.[34] However, sensible heat flux was negative throughout most of the whole day after March 24, mainly because the surface temperature was overestimated in the daytime when the snow had melted completely. LE was negative throughout most of the experiment period, but was close to zero after March 24 [Fig. 7(b)], indicating that the release of latent heat of vaporization

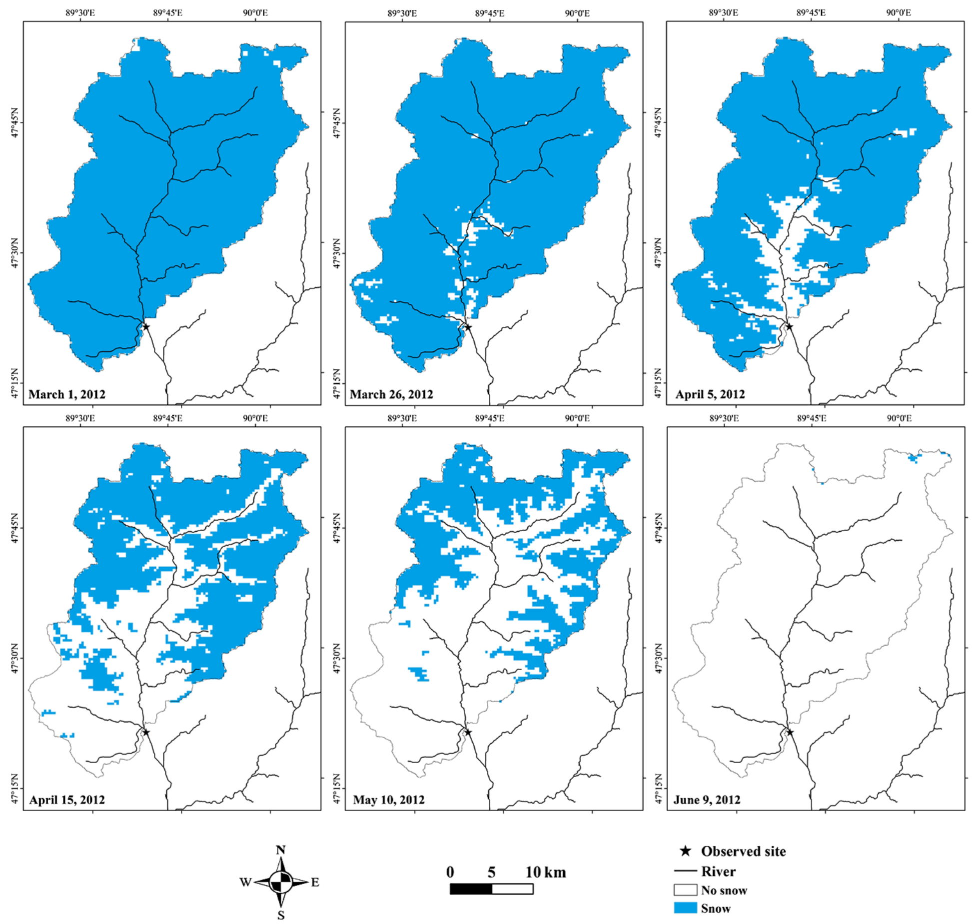

Fig. 4 Mapping of snow cover variations in spring in Kayiertesi River Basin.

became weak when the snow melted completely. The daily mean values of LE varied between -15.5 and -3 W/m^2 when the ground was covered by snow. The net radiation followed an orderly daily cycle but significantly increased after the snow disappeared. R_n remained positive in the daytime and negative at night during the experiment period, with variations of daily mean values between -22.4 and 106 W/m^2. The monthly mean of R_n was 35 W/m^2 in March, suggesting that it was the major energy source of the snowmelt.

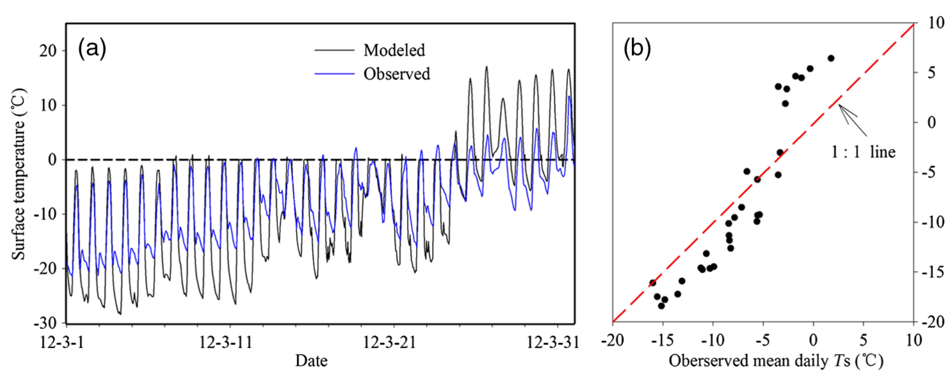

Fig. 5 (a) Comparison between modeled and observed surface temperature, (b) scatter plot between the modeled and observed mean daily surface temperature.

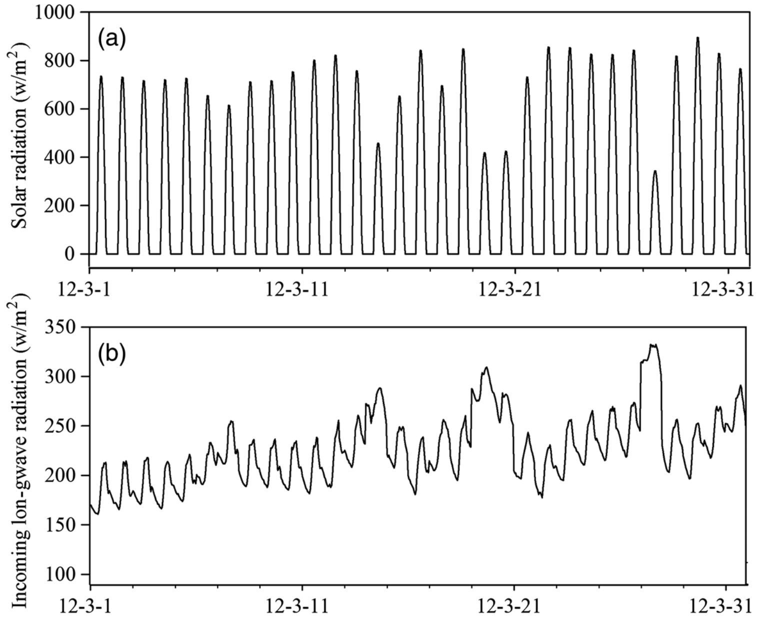

Fig. 6 (a) Hourly incoming short-wave and (b) long-wave radiations variation from March 1 1:00 a.m. to April 1 0:00 a.m.

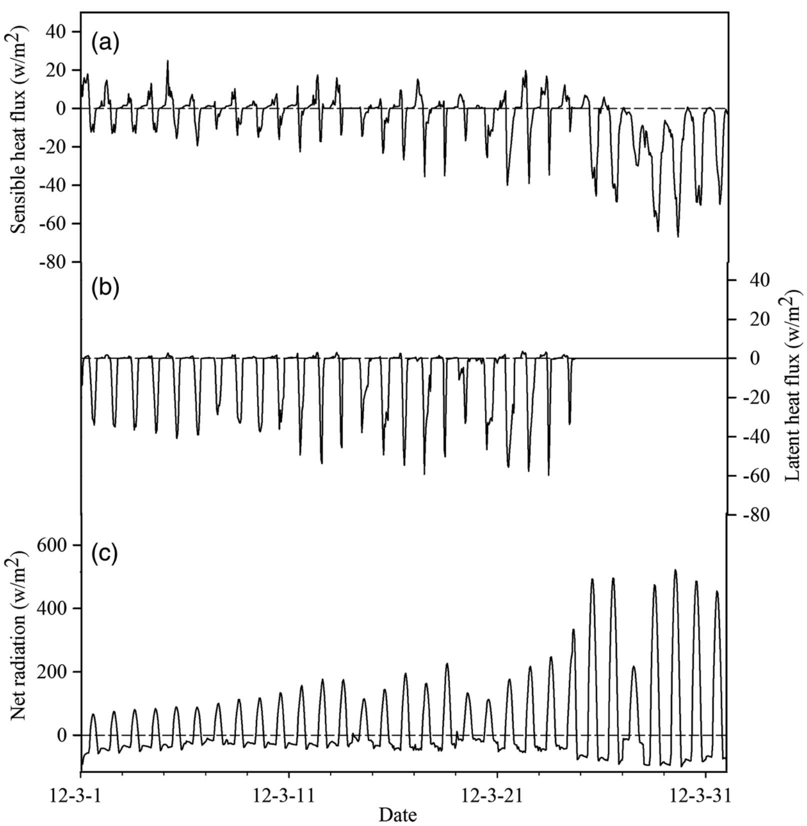

Fig. 7 Hourly surface energy fluxes variation during the simulation period. (a) Sensible heat flux, (b) latent heat flux, and (c) net radiation.

4.4 *Snowmelt Outflow*

When the water-holding capacity of snow is exceeded by the snow liquid water content, excess liquid water will move down under the action of gravity and will finally flow out from the snow layer. The modeled outflow during the snowmelt period is shown in Fig. 8. Outflow began after March 16, which was half a month after the snow melt began. This occurred because net energy is first used to increase the temperature in the snow layer. Only after the input net energy satisfies the internal energy of the snow layer and reaches the boundary conditions of snow melting can the rest of the energy be used to melt the snow layer. However, not all of the snowmelt water will immediately convert to outflow when snow melting occurs, due to the water-holding capacity of the snow layer. When the snow layer saturated with water content, outflow will occur.

There were two continuous rapid snowmelt processes in the spring of 2012 at the experiment site. The first occurred on March 16 to 19. From March 1 to 15, the snow melt rate stayed very low and the outflow was negligible. By March 16, the temperature began to increase rapidly, reaching a maximum of 4.88°C on March 18. Continued warming created conditions for snow melting and the outflow rose from March 16 onward. By March 18, the outflow had reached 1.51 $\text{mm}\,\text{h}^{-1}$. From March 19 onward, significant cooling occurred for 3 days and the temperature decreased until March 22 (Fig. 2). According to the observational data, there was 0.1 mm w.e. of precipitation on March 19, which was the only instance of snowfall in the month. As a result, the outflow was very low at that time and there was no strong snow melting. From March 22 onward, the air temperature rose again, reaching 3.9°C at 1:00 p.m. on March 23 and 6.4°C by noon on March 24. After that, the air temperature remained above 0°C throughout most of the days. Therefore, the next strong snowmelt process appeared on March 22 to 24, with a peak outflow value of 6.3 $\text{mm}\,\text{h}^{-1}$ at 2:00 p.m. on March 24, indicating that the higher temperature caused rapid snow melting. The peak outflow value was very close to the results at a study site of Tianshan, Xinjiang, which had a peak snowmelt outflow value of 5.8 $\text{mm}\,\text{h}^{-1}$ in March 2009.[35]

To validate the outflow results, we compared the snowmelt process (as revealed by outflow) with the process of SWE (Fig. 8). The SWE decreased drastically from March 18 to 20 and from March 23 to 25. The dates of these large reductions of SWE corresponded to the times when strong outflow was occurring, which demonstrates that large snowmelt outflow occurs when snow is melting rapidly. This also suggests that our modeled snowmelt outflow was reasonable. To further quantitatively verify the accuracy of the outflow model, we calculated the water balance for the entire month of March. Based on the mass conservation principle, snowmelt outflow and sublimation increase with a decrease of the amount of snow, and the amount of snow will increase when there is snowfall. In this study, snowmelt outflow and sublimation were defined as water loss during snow melting; initial SWE, precipitation, and condensation were defined as obtained water. During the period of snow melting, the initial SWE was 0.0605 m from observational data, the precipitation was 0.0001 m w.e., the total water loss of outflow derived from the model was 0.05419 m w.e. and the water loss from sublimation was 0.00586 m w.e. (condensation had been deducted). The total water loss (0.06005 m w.e.) calculated using the model

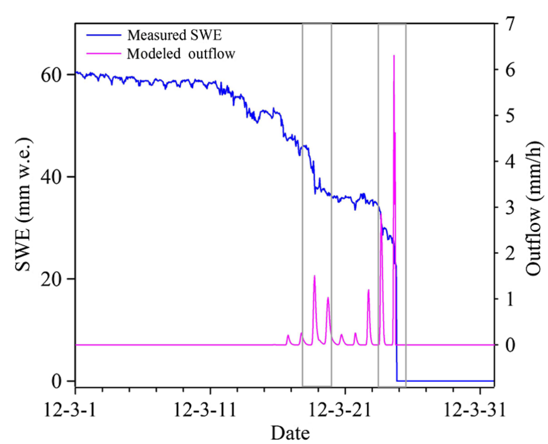

Fig. 8 Map of simulated snowmelt outflow in snow layer.

matched perfectly with the obtained water (0.0606 m w.e.) from measurements. This implied that the water amount remained balanced during the modeled period. From this viewpoint, the modeled outflow can be considered credible.

5 Conclusions

This study evaluated the feasibility of using the UEB model to simulate the melt process of snow cover in the Kayiertesi River Basin in the Altay Mountains of Xinjiang, and to model the SWE, in order to forecast peak snowmelt outflows during the spring season. The modeled results were validated by field measurements, remotely sensed data, and existing researches. We also assessed surface energy flux and snowmelt outflow, and drew the following conclusions:

1. The UEB model can be considered a feasible tool to predict snowmelt processes in mountain basins of northwestern China. The main snowmelt process was well modeled, with a mean relative error of 7.2% in modeling the SWE variation at the Kuwei observation site.
2. The studied snowmelt process lasted for 24 days; net radiation was the major input energy source of snowmelt during the period. The snowmelt outflow was closely related to air temperature and snowmelt amounts; the peak outflow appeared on March 24 with the value of 6 $\mathrm{mm\,h^{-1}}$ on the site.

The results of this study can enhance the understanding of rapid snowmelt processes and energy variation. It also can provide a baseline reference for simulated snowmelt distributions in mountain basins of northwestern China. Future work that should be done in this specific mountain basin is to predict rapid snowmelt rates based on remote sensing data using the UEB model and the calibrated parameters that were used in this study. Model improvement is still necessary for better prediction of snowmelt processes, and data from four new radiometers that were installed at the Kuwei observation site in 2013 will serve as an observational check for future the more model results, including atmospheric radiation.

Acknowledgments

This work was supported by the National Key Research Program of Global Change Research (Grant No. 2010CB951404), the National Science Fundamental Key Project (Grant Nos. 41190084, 41271083, and 41201062). We also thank the journal's anonymous reviewers and the journal's editor, whose comments and suggestions helped us to improve the quality of this paper.

References

1. A. E. Tekeli et al., "Using MODIS snow cover maps in modeling snowmelt runoff process in the eastern part of Turkey," *Remote Sens. Environ.* **97**(2), 216–230 (2005), http://dx.doi.org/10.1016/j.rse.2005.03.013.
2. Y. P. Shen et al., "The responses of glaciers and snow cover to climate change in Xinjiang (II): hazards effects," *J. Glaciol. Geocryol.* **35**(06), 1355–1370 (2013) (in Chinese).
3. P. Qiao, Y. Qin, and Z. Liu, "A spatially distributed snowmelt model based on energy balance," *J. China Hydrol.* **31**(03), 22–26+35 (2011) (in Chinese).
4. N. Reeh, "Parameterization of melt rate and surface temperature on the Greenland ice sheet," *Polarforschung* **59**(3), 113–128 (1989).
5. R. Hock, "A distributed temperature-index ice-and snowmelt model including potential direct solar radiation," *J. Glaciol.* **45**(149), 101–111 (1999).
6. A. Semádeni-Davies, "Monthly snowmelt modelling for large-scale climate change studies using the degree-day approach," *Ecol. Model.* **101**(2), 303–323 (1997), http://dx.doi.org/10.1016/S0304-3800(97)00054-9.

7. H. Ma, Z. Liu, and Y. Liu, "Energy balance of a snow cover and simulation of snowmelt in the western Tien Shan Mountains, China," *Ann. Glaciol.* **16**, 73–78 (1991).
8. S. Liu et al., "Mass balance of Kangwure (flat-top) Glacier on the north side of Mt. Xixiabangma, China," *Bull. Glacier Res.* **14**, 37–43 (1996).
9. R. J. Braithwaite and Y. Zhang, "Sensitivity of mass balance of five Swiss glaciers to temperature changes assessed by tuning a degree-day model," *J. Glaciol.* **46**(152), 7–14 (2000), http://dx.doi.org/10.3189/172756500781833511.
10. G. Jost et al., "Distributed temperature-index snowmelt modelling for forested catchments," *J. Hydrol.* **420–421**, 87–101 (2012), http://dx.doi.org/10.1016/j.jhydrol.2011.11.045.
11. J. Martinec and A. Rango, "Parameter values for snowmelt runoff modelling," *J. Hydrol.* **84**(3), 197–219 (1986), http://dx.doi.org/10.1016/0022-1694(86)90123-X.
12. N. A. Abebe, F. L. Ogden, and N. R. Pradhan, "Sensitivity and uncertainty analysis of the conceptual HBV rainfall-runoff model: implications for parameter estimation," *J. Hydrol.* **389**(3), 301–310 (2010), http://dx.doi.org/10.1016/j.jhydrol.2010.06.007.
13. R. Hock, "Temperature index melt modelling in mountain areas," *J. Hydrol.* **282**(1), 104–115 (2003), http://dx.doi.org/10.1016/S0022-1694(03)00257-9.
14. K. Brubaker, A. Rango, and W. Kustas, "Incorporating radiation inputs into the snowmelt runoff model," *Hydrol. Processes* **10**(10), 1329–1343 (1996), http://dx.doi.org/10.1002/(ISSN)1099-1085.
15. P. Bartelt and M. Lehning, "A physical SNOWPACK model for Swiss avalanche warning, Part I: numerical model," *Cold Reg. Sci. Technol.* **35**(3), 123–145 (2002), http://dx.doi.org/10.1016/S0165-232X(02)00074-5.
16. J. Pomeroy, D. Gray, and P. Landine, "The prairie blowing snow model: characteristics, validation, operation," *J. Hydrol.* **144**(1), 165–192 (1993), http://dx.doi.org/10.1016/0022-1694(93)90171-5.
17. G. Flerchinger and K. Saxton, "Simultaneous heat and water model of a freezing snow-residue-soil system, II: field verification," *Trans. ASAE* **32**(2), 573–578 (1989), http://dx.doi.org/10.13031/2013.31041.
18. V. Mahat, D. G. Tarboton, and N. P. Molotch, "Testing above- and below-canopy representations of turbulent fluxes in an energy balance snowmelt model," *Water Resour. Res.* **49**(2), 1107–1122 (2013), http://dx.doi.org/10.1002/wrcr.20073.
19. V. Mahat and D. G. Tarboton, "Correction to 'Canopy radiation transmission for an energy balance snowmelt model'," *Water Resour. Res.* **48**(3), W01534 (2012), http://dx.doi.org/10.1029/2012WR011964.
20. M. B. Abbott et al., "An introduction to the European Hydrological System (Système Hydrologique Européen, SHE), 1: history and philosophy of a physically-based, distributed modelling system," *J. Hydrol.* **87**(1), 45–59 (1986), http://dx.doi.org/10.1016/0022-1694(86)90114-9.
21. R. Srinivasan and J. G. Arnold, "Integration of a basin-scale water quality model with GIS," *J. Am. Water Resour. Assoc.* **30**(3), 453–462 (1994), http://dx.doi.org/10.1111/jawr.1994.30.issue-3.
22. M. S. Wigmosta, L. W. Vail, and D. P. Lettenmaier, "A distributed hydrology-vegetation model for complex terrain," *Water Resour. Res.* **30**(6), 1665–1679 (1994), http://dx.doi.org/10.1029/94WR00436.
23. X. Zhou, H. Xie, and J. M. Hendrickx, "Statistical evaluation of remotely sensed snow-cover products with constraints from streamflow and SNOTEL measurements," *Remote Sens. Environ.* **94**(2), 214–231 (2005), http://dx.doi.org/10.1016/j.rse.2004.10.007.
24. X. Huang et al., "Validation of MODIS snow cover products using Landsat and ground measurements during the 2001–2005 snow seasons over northern Xinjiang, China," *Int. J. Remote Sens.* **32**(1), 133–152 (2011), http://dx.doi.org/10.1080/01431160903439924.
25. D. G. Tarboton, T. G. Chowdhury, and T. H. Jackson, "A spatially distributed energy balance snowmelt model," in *Proc. of a Boulder Symposium Biogeochemistry of Seasonally Snow-Covered Catchments*, K. A. Tonnessen, M. W. Williams, and M. Tranter, Eds., pp. 228, IAHS Publ., Boulder, Colorado (1994).
26. D. G. Tarboton and C. H. Luce, "Utah energy balance snow accumulation and melt model (UEB): computer model technical description and users guide," Utah Water

Research Laboratory and USDA Forest Service Intermountain Research Station, Utah (1996).
27. R. E. Dickinson, A. Henderson-Sellers, and P. J. Kennedy, "Biosphere-atmosphere transfer scheme (BATS) v. 1e as coupled to the NCAR community climate model," Tech. Note NCAR/TN-387+STR, pp. 21, National Center of Atmospheric Research, Boulder, Colorado (1993).
28. K. L. Bristow and G. S. Campbell, "On the relationship between incoming solar radiation and daily maximum and minimum temperature," *Agric. For. Meteorol.* **31**(2), 159–166 (1984), http://dx.doi.org/10.1016/0168-1923(84)90017-0.
29. T. Jackson, "A spatially distributed snowmelt-driven hydrologic model applied to Upper Sheep Creek," PhD Dissertation, Utah State University, Logan, Utah (1994).
30. D. Male, "Snowcover ablation and runoff," in *Handbook of Snow*, D. Male and D. Gray, Eds., pp. 360–436, Pergamon Press, Toronto (1981).
31. W. Yang et al., "Summertime surface energy budget and ablation modelling in the ablation zone of a maritime Tibetan glacier," *J. Geophys. Res.* **116**(D14), D14116 (2011), http://dx.doi.org/10.1029/2010JD015183.
32. W. Sun et al., "Surface energy balance in the accumulation zone of the Laohugou Glacier No. 12 in the Qilian Mountains during ablation period [in Chinese]," *J. Glaciol. Geocryol.* **33**(1), 38–45 (2011).
33. J. Yao et al., "The surface energy budget and evapotranspiration in the Tanggula region on the Tibetan Plateau," *Cold Reg. Sci. Technol.* **52**(3), 326–340 (2008), http://dx.doi.org/10.1016/j.coldregions.2007.04.001.
34. H. Jiang, K. Wang, and G. Wu, "Effects of surface temperature and its taking values on atmospheric longwave radiation cooling over the QingHai-Xizang Plateau [in Chinese]," *Plateau Meteorol.* **16**(03), 27–34 (1997).
35. Z. C. Wei, "The study on snow melt processes simulation and snow characteristics analysis [in Chinese]," Master's Thesis, Xinjiang Univ., Urumchi, Xinjiang (2010).

Xuejiao Wu is a PhD student at Cold and Arid Regions Environmental and Engineering Research Institute (CAREERI), Chinese Academy of Sciences (CAS). She received her Master of Science degree in cartography and geography information system from CAREERI, CAS in Lanzhou in 2012. Her research interest is GIS and remote sensing application, especially on snow modeling and snowmelt flood forecasting.

Ninglian Wang is a professor at Cold and Arid Regions Environmental and Engineering Research Institute, Chinese Academy of Sciences. He received the Excellent Prize for Top 100 Ph.D. Dissertations, Ministry of Education of the Peoples' Republic China in 2004 and the Honor of Outstanding Young Scientists, Chinese NSF in 2005. His research fields include climatic and environmental records in ice cores, the cryosphere, water resources and global change and the solar activity and the Earth climate change.

Yongping Shen is a professor at Cold and Arid Regions Environmental and Engineering Research Institute, Chinese Academy of Sciences. His expertise is in glacial hydrology and water resources, the effects of climate change on water resources and the snow disaster formation mechanism research.

Jianqiao He received his PhD degree from Cold and Arid Regions Environmental and Engineering Research Institute (CAREERI), Chinese Academy of Sciences (CAS). He is a research assistant of State Key Laboratory of Cryospheric Sciences, CAREERI, CAS. His work is focused on the study of glacier and global change, isotope hydrology.

Wei Zhang is a PhD student at the Cold and Arid Regions Environmental and Engineering Research Institute, Chinese Academy of Sciences. He received his bachelor's degree in hydrology and water resources engineering and master's degree in hydrology and water resources from Lanzhou University in 2010 and 2013, respectively. His research interests include snow hydrology, permafrost hydrology, and cold region hydrological models.